Gate-dependent spin-orbit coupling in multielectron carbon nanotubes

Jespersen, Thomas Sand; Grove-Rasmussen, Kasper; Paaske, Jens; Muraki, K.; Fujisawa, T.; Nygård, Jesper; Flensberg, Karsten

Published in:
Nature Physics

DOI:
10.1038/NPHYS1880

Publication date:
2011

Document version
Early version, also known as pre-print

Gate-Dependent Orbital Magnetic Moments in Carbon Nanotubes

T. S. Jespersen,[1,*] K. Grove-Rasmussen,[1,2,*] K. Flensberg,[1] J. Paaske,[1] K. Muraki,[2] T. Fujisawa,[3] and J. Nygård[1]

[1]*Niels Bohr Institute & Nano-Science Center, University of Copenhagen, Universitetsparken 5, DK-2100 Copenhagen, Denmark*

[2]*NTT Basic Research Laboratories, NTT Corporation, 3-1 Morinosato-Wakamiya, Atsugi 243-0198, Japan*

[3]*Research Center for Low Temperature Physics, Tokyo Institute of Technology, Ookayama, Meguro, Tokyo 152-8551, Japan*

(Received 19 May 2011; published 25 October 2011)

We investigate how the orbital magnetic moments of electron and hole states in a carbon nanotube quantum dot depend on the number of carriers on the dot. Low temperature transport measurements are carried out in a setup where the device can be rotated in an applied magnetic field, thus enabling accurate alignment with the nanotube axis. The field dependence of the level structure is measured by excited state spectroscopy and excellent correspondence with a single-particle calculation is found. In agreement with band structure calculations we find a decrease of the orbital magnetic moment with increasing electron or hole occupation of the dot, with a scale given by the band gap of the nanotube.

DOI: 10.1103/PhysRevLett.107.186802 PACS numbers: 73.63.Fg, 73.23.Hk, 73.63.Kv

The response of an electron in a quantum dot to an applied magnetic field is determined by the coupling to the electron spin—the Zeeman effect—and the coupling to the orbital magnetic moment of the electron. In carbon nanotubes the electrons encircle the circumference of the tube with a resulting magnetic moment pointing along the nanotube axis which thus couples to the parallel component of an applied magnetic field. This was first studied by Minot *et. al.* [1], for the first few carriers in small band-gap nanotubes where the resulting orbital g factor, g_{orb} was shown to reflect the nanotube diameter. Recently, the surprising discovery of a strong spin-orbit interaction in nanotubes [2–10] has spurred renewed interest in the use of carbon nanotubes as templates for spin qubits addressable by electric fields [11,12]. One new possibility is to control the spin-orbit magnetic field and the parallel component of an applied magnetic field by moving the quantum dot along a curved nanotube segment [13].

This calls for a better understanding of the relation between the nanotube band structure and the inherited properties of nanotube quantum dots. Here we extend the work of Ref. [1] by investigating the dependence of g_{orb} on the electron or hole occupation of a nanotube quantum dot tuned by a potential V_g on a nearby electrostatic gate. We find g_{orb} decreasing with electron or hole filling as the circumferential velocity of the electrons decrease and we show that while the nanotube diameter determines the value of g_{orb} for the first carrier, the nanotube band gap Δ_g sets the scale of its gate dependence.

It is well established that the low energy electron dispersion for nanotubes can be obtained from the graphene dispersion by imposing periodic boundary conditions in the circumferential direction of the nanotube [14]. Ignoring spin-orbit effects this leads to $E(k_\parallel) = \pm\hbar v_F\sqrt{k_g^2 + k_\parallel^2}$, where $v_F \simeq 10^6$ m/s is the Fermi velocity of graphene, $k_{||}$ is the component of the wave vector along the nanotube axis and the offset k_g between the quantization lines and the Dirac points of the graphene dispersion, results in a band gap $\Delta_g = \hbar v_F k_g$ for the nanotube [15]. A magnetic field $B_\parallel$ applied parallel to the nanotube axis adds an Aharonov-Bohm phase to the electron wave function and shifts the circumferential quantization lines by $k_\Phi = eB_\parallel D/4\hbar$ where D is the nanotube diameter. Letting $s = \pm 1$ denote the spin $\uparrow, \downarrow$ along the nanotube and $\tau = \pm 1$ the corner points K, K' of the graphene Brillouin zone, the dispersion reads

$$E_{\tau,s} = \pm\hbar v_F\sqrt{(\tau k_\Phi - k_g)^2 + k_\parallel^2} + \frac{1}{2}s g_s \mu_B B, \quad (1)$$

where $g_s = 2$ and the last term accounts for the usual Zeeman effect. Including explicitly the angle θ between the nanotube axis and the applied field and expanding to linear order in B leads to [16]

$$E_{\tau,s} \approx E_0^{\pm} + \left(\frac{1}{2}g_s s \mp \tau g_{\mathrm{orb}}\cos(\theta)\right)\mu_B B, \quad (2)$$

with $E_0^{\pm} = \pm\sqrt{\Delta_g^2 + \varepsilon_N^2}$ and

$$g_{\mathrm{orb}} = \frac{e v_F D}{4\mu_B\sqrt{1 + (\frac{\varepsilon_N}{\Delta_g})^2}}. \quad (3)$$

Here the result has been written for a nanotube quantum dot with electrons confined to a nanotube segment of length L where $\varepsilon_N = \hbar v_F N\pi/L$. Experimentally verifying Eq. (3) is the main objective of this work. For the first carriers $\varepsilon_N \ll \Delta_g$, yielding $g_{\mathrm{orb}} \approx e v_F D/4\mu_B$ which is the value classically expected for an electron in a circular motion of diameter D and speed v_F [1]. For increasing electron or hole occupation of the dot (larger ε_N) g_{orb} decreases as shown in Fig. 1(a) with a characteristic scale set by the band gap Δ_g. This behavior arises from the graphene dispersion as schematically illustrated in the inset and in Fig. 1(b): Because of the linear dispersion, v_F does not depend on energy (black arrows) and thus the

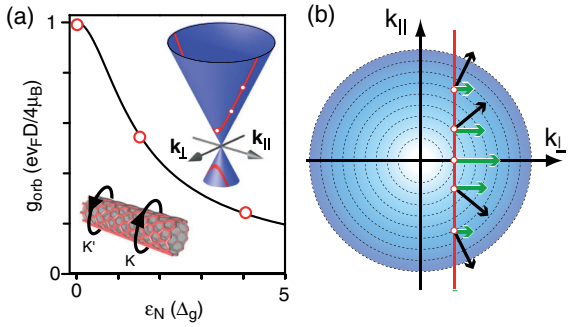

FIG. 1 (color online). (a) Dependence of $g_{\rm orb}$ on the energy ε_N of the Nth-longitudinal electron mode of the nanotube quantum dot. $g_{\rm orb}$ has been normalized by $ev_F D/4\mu_B$ expected for the first electron on the nanotube and ϵ_N are displayed in units of the band gap Δ_g. (b) Contour plot of the graphene Dirac dispersion around a K point of the Brillouin zone [upper right inset in (a)]. The first nanotube band is obtained by cutting at constant $k_\perp = k_g$ (red curve in inset). Black and green (horizontal) arrows illustrate the constant Fermi velocity $\nabla_k E$ and the circumferential velocity $\partial E/\partial k_\perp$ decreasing with increasing $k_\parallel$.

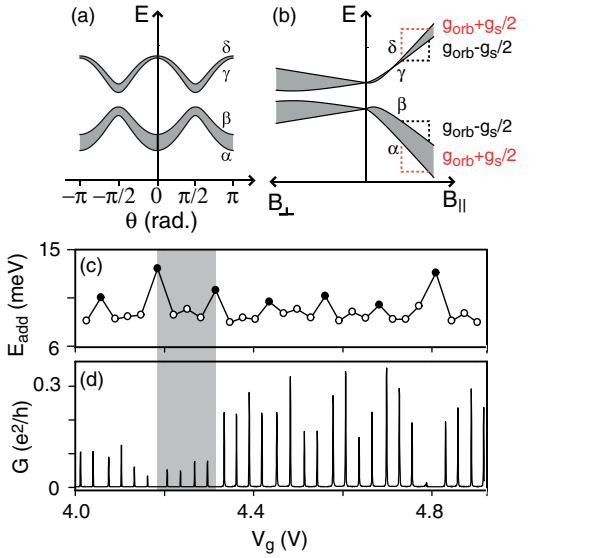

FIG. 2 (color online). (a) Evolution of the level quartet upon rotation of the nanotube in a constant magnetic field. The model contains both disorder and spin-orbit coupling. (b) Field dependence of the energy levels in the perpendicular and parallel orientation. (d) Coulomb peaks of a nanotube quantum dot measured at 100 mK. The fourfold periodicity of the spectra is evident in the addition energies (c).

circumferential component of the velocity (green horizontal arrows), which determines $g_{\rm orb}$, decreases as electrons with a larger parallel component are added.

To measure $g_{\rm orb}(N)$ and investigate the relationship of Eq. (3) we have performed level spectroscopy on a nanotube quantum dot at different occupations. Equation (2) contains the well established fourfold degenerate nanotube level structure [17,18]: a factor of 2 from ordinary spin ($s = \pm 1$) and a factor of 2 from the isospin degeneracy ($\tau = \pm 1$) of clockwise, K, and anticlockwise, K', orbits [Fig. 1(a) inset]. In real devices the degeneracy is generally split by a combination of spin-orbit coupling $\Delta_{\rm SO}$ [2,5,19] (which favors parallel or antiparallel alignment of orbital and spin magnetic moments) and disorder scattering $\Delta_{KK'}$ (which couples K and K' states). Figures 2(a) and 2(b) show the evolution of the single-particle spectrum upon rotation of the nanotube in a constant field and as a function of field strength for the perpendicular ($B_\perp$) and parallel ($B_\parallel$) orientations. The coupling of the parallel magnetic field to the orbital magnetic moment results in the steep slopes in $B_\parallel$, and $g_{\rm orb}$ can be determined as indicated. Three parameters thus characterize the level structure: $\Delta_{KK'}$, $\Delta_{\rm SO}$, and $g_{\rm orb}$. In Ref. [5], we analyzed the role of $\Delta_{\rm SO}$ and now we focus on the orbital magnetic moment extracted from the same set of data.

Our experimental setup is as follows: High-quality single-wall carbon nanotubes are grown by chemical vapor deposition from catalyst islands predefined on substrates of highly doped silicon capped with an insulating oxide. Subsequently paladium/gold (10 nm/40 nm) source and drain contact electrodes are defined by electron beam lithography with a spacing of 400 nm that defines the nanotube segment constituting the quantum dot. The electron or hole occupancy of the quantum dot can be tuned by applying a voltage V_g to the conducting backplane of the substrate and we characterize the quantum dot by measuring the two-terminal differential conductance $dI/dV_{\rm sd}$ or transconductance dI/dV_g by standard lock-in techniques; here $V_{\rm sd}$ is the applied source-drain voltage and I the resulting current. The sample is measured at a temperature of $\sim$100 mK in a dilution refrigerator fitted with a 9 T superconducting magnet and a piezorotator [20] allowing full in-plane rotation of the sample.

Figure 2(d) shows the linear conductance G of the device as a function of V_g revealing a series of peaks characteristic of a quantum dot in the Coulomb blockade regime [21]. In the valleys of low conductance the number of electrons on the quantum dot n is fixed and with increasing V_g a peak emerges when the next charge state $(n + 1)$ becomes available for transport. The peak separations, which are extracted in Fig. 2(c), measure the energy, $E_{\rm add}$, required for adding the next electron. This energy is the combination of the constant electrostatic charging energy and the energy spacing of the quantum levels of the dot. As seen in the figure, $E_{\rm add}$ is fourfold periodic reflecting the near fourfold degenerate level structure discussed above. In the following, we present the details of the measurements of $g_{\rm orb}$ in the highlighted quartet.

Figure 3(a) shows the measured transconductance dI/dV_g as a function of applied bias $V_{\rm sd}$ and V_g of the shaded quartet in Figs. 2(c) and 2(d) corresponding to $n_0 \simeq 120$ electrons occupying the quantum dot. The diamond shaped zero conductance regions are characteristic for a quantum dot in the Coulomb blockade regime

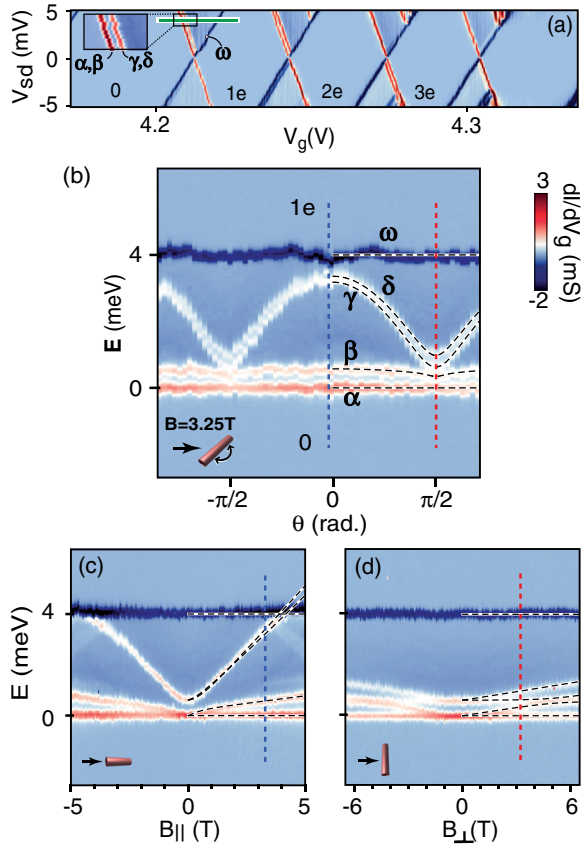

FIG. 3 (color online). (a) Measured transconductance dI/dV_g around the first electron of the shaded quartet in Figs. 2(c) and 2(d). (b) dI/dV_g vs V_g for $V_{sd} = 4$ mV along the green horizontal line in (a) measured in a constant magnetic field $B = 3.25$ T while rotating the sample. The black and white dashed lines are a fit to the single-particle model. The leftmost (rightmost) vertical line indicates parallel (perpendicular) alignment with the applied field. (c), (d) As (b) but measured in a parallel and perpendicular magnetic field, respectively. The fits in (b)–(d) yield $g_{orb} = 7.8$. In (b)–(d) an overall magnetic field dependent shift of the ground states are compensated, and the theoretical fits are only partly overlaid not to mask the underlying data.

where transport occurs through sequential tunneling of electrons and excited states appear as high-conductance lines parallel to the diamond edges. We focus on the states of the first electron, i.e., the lines terminating at the $1e$ diamond, enhanced in the inset. The lines are labeled using the terminology of Figs. 2(a) and 2(b). Since transconductance rather than dI/dV_{sd} is measured, the lines acquire a sign depending on whether they correspond to levels entering or leaving the bias window [21]. This feature eases the identification of the lines in Fig. 3(b) where we show traces along the green horizontal line in Fig. 3(a) ($V_{sd} = 4$ mV) while applying a fixed magnetic field $B = 3.25$ T and rotating the sample [22]. In agreement with Fig. 2(a) the diamond edge in Fig. 3(a) has split into two lines: the ground state (labeled α) and the excited state β. Also the line of the excited state in Fig. 3(a) is composed of two individual states (γ, and δ), and the separation between this doublet and the ground state exhibits a strong oscillating dependence on the orientation of the sample. This behavior agrees with the θ dependence of Eq. (2), and allows us to determine the orientation of the nanotube axis relative to the applied field ($\theta = 0$ for parallel alignment). This is crucial for an accurate measurement of g_{orb}. The zero-field splitting of the ground state into two doublets is a result of a combination of the $\Delta_{KK'}$ and Δ_{SO} as discussed above. Further, from Eq. (2) the internal splittings of the two doublets $\tau = 1$, $s = \mp 1$, (α, β) and $\tau = -1$, $s = \mp 1$ (γ, δ) should both equal the Zeeman splitting $g_s \mu_B B$, however, this is clearly not the case in the measurement: the (α, β) doublet exhibits a larger splitting than the excited doublet, and while the (α, β) splitting slightly decreases close to the perpendicular orientation of the field, $\theta = \pm\pi/2$, the (β, γ) splitting slightly increases. This asymmetry is an effect of the spin-orbit interaction and, as illustrated by the dashed lines, the measurement is in near perfect agreement with the result of the single-particle calculation with parameters $\Delta_{KK'} = 0.58$ meV, $\Delta_{SO} = 0.2$ meV, and $g_{orb} = 7.8$. Importantly, in this way we have accurately determined the orbital g factor. With these parameters fixed, the level structure is, within the single-particle model, completely determined. For consistency we show in Figs. 3(c) and 3(d) the measurement of the level structure as a function of $B_{||}$ and $B_{\perp}$, respectively: The measurements agree perfectly with the model, with no free parameters. In the case of the parallel field the coupling to the orbital motion results in the steep sloping of the excited doublet while $B_{\perp}$ does not couple to the orbital motion and the two doublets split equally [cf. Fig. 2(b)].

To investigate the gate dependence of g_{orb} we repeat this analysis for quartets at different occupation (spectroscopic data in supplement of Ref. [5]). Figure 4 shows the gate dependence of the resulting values and values extracted from the $B_{||}$ dependence of zero-bias Coulomb peaks [1] (see Supplemental Material [23]). Clearly, g_{orb} decreases as electrons or holes are added to the conduction or valence band confirming the decrease of the orbital magnetic moment for states further away from the band edge as predicted by Eq. (3). This is the main result of our work. The solid line shows a fit to Eq. (3) with the diameter D and Δ_g as the free parameters [24]. The fit is in reasonable agreement with the measurement and yields a band gap of 23 meV in good agreement with the gap estimate of $\sim$15 meV from the measured stability diagram (see Supplemental Material [23]). The fit, however, yields a diameter of $D = 5.3$ nm, which is unrealistically large for nanotubes grown by chemical vapor deposition which are expected to have $D \lesssim 3$ nm. Unexpectedly large diameters are also inferred in other spectroscopic studies [1,2,25,26]; e.g., Kuemmeth *et al.* found a diameter of $D \simeq 5$ nm [2]. Yet other reports find more reasonable

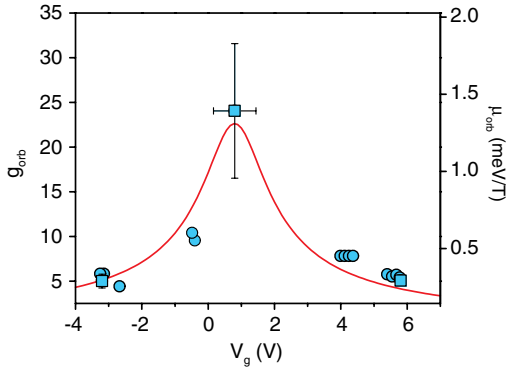

FIG. 4 (color online). g_{orb} and corresponding orbital magnetic moments $\mu_{orb} = g_{\mathrm{orb}}\mu_B$ as a function of gate, showing a decrease with electron or hole filling. Values are extracted from excited state spectroscopy (○) and Coulomb peak dependence on $B_{\parallel}$ (□). Close to the band gap a clear fourfold periodicity is absent impeding direct comparison to the model. Instead g_{orb} was measured for all charge states in the region indicated by the horizontal error bar with a spread in values indicated by the vertical error bar. The line is a fit to Eq. (3) assuming a constant dot length and with $\epsilon_N(V_g) \propto (V_g - 0.8\ \mathrm{V})$ yielding $D = 5.3$ nm and $\Delta_g = 23$ meV.

diameters $D \simeq 1.5$ nm [1,27–29]. We have considered various explanations for this finding. First, as seen from Eq. (3) the estimated diameter depends on the Fermi velocity. For flat graphene v_F may be strongly enhanced by interactions [30]; however, for finite sized nanotubes this effect is expected to be small, and the spread in experimentally determined values (0.82–1.1×10^6 m/s) [31,32] is too small to account for our findings. Second, our model assumes a constant length of the quantum dot, i.e., $\epsilon_N \propto V_g$. Because of the screening of the back gate field by the contacts a decreased dot size could be expected for small N. Extending the model with a gate-dependent effective dot length, however, further increases the estimated diameter and thus does not explain the result. To resolve this discrepancy, additional experimental work is needed measuring $g_{\mathrm{orb}}(N)$ in nanotubes with independently determined diameters and band gaps, e.g., combining transport with Raman spectroscopy [33].

Establishing the exact theoretical relationship between g_{orb} and electron filling would be very valuable as it may allow for an accurate determination of both diameter and band-gap parameters that could then be used for assigning the chirality of the nanotube from transport measurements alone. Furthermore, within the present theory, the gate dependence of g_{orb} is identical to the gate-dependent part of the curvature induced spin-orbit interaction [5]. Thus the experimentally more accessible parameter g_{orb} can be used to infer information about the less accessible, but very important, spin-orbit interaction. This may prove useful for future utilizations of the spin-orbit interaction as the means of manipulating spins in nanotube quantum dots.

In conclusion, we have investigated the gate dependence of the orbital magnetic moment of quantum states in high-quality carbon nanotube quantum dots. We present low temperature transport measurements of the dependence of quantum state energies on the angle between the nanotube axis and an applied magnetic field. This allows the determination of the nanotube axis from transport measurements alone and an accurate value for the orbital g factor is found by comparison with a single-particle model taking into account both disorder-scattering and spin-orbit interaction. Repeating such measurement over a wide range of gate voltages we find that the orbital magnetic moment decreases with dot occupation in agreement with the expectations from band structure considerations.

We thank P. E. Lindelof, J. Mygind, H. I. Jørgensen, C. M. Marcus, and F. Kuemmeth for discussions and experimental support. T. S. J. acknowledges the Carlsberg Foundation and Lundbeck Foundation for financial support. K. G. R., K. F., and J. N. acknowledge The Danish Research Council and University of Copenhagen Center of Excellence.

*tsand@fys.ku.dk

[1] E. Minot *et al.*, Nature (London) **428**, 536 (2004).
[2] F. Kuemmeth *et al.*, Nature (London) **452**, 448 (2008).
[3] H. Churchill *et al.*, Nature Phys. **5**, 321 (2009).
[4] F. Kuemmeth *et al.*, Mater. Today **13**, 18 (2010).
[5] T. Jespersen *et al.*, Nature Phys. **7**, 348 (2011).
[6] T. Ando, J. Phys. Soc. Jpn. **69**, 1757 (2000).
[7] L. Chico, M. P. Lopez-Sancho, and M. C. Munoz, Phys. Rev. Lett. **93**, 176402 (2004).
[8] D. Huertas-Hernando, F. Guinea, and A. Brataas, Phys. Rev. B **74**, 155426 (2006).
[9] J. S. Jeong and H. W. Lee, Phys. Rev. B **80**, 075409 (2009).
[10] W. Izumida, K. Sato, and R. Saito, J. Phys. Soc. Jpn. **78**, 074707 (2009).
[11] D. V. Bulaev, B. Trauzettel, and D. Loss, Phys. Rev. B **77**, 235301 (2008).
[12] J. Klinovaja *et al.*, Phys. Rev. Lett. **106**, 156809 (2011).
[13] K. Flensberg and C. M. Marcus, Phys. Rev. B **81**, 195418 (2010).
[14] R. Saito, G. Dresselhaus, and M. Dresselhaus, *Physical Properties of Carbon Nanotubes* (Imperial College Press, London, 1998).
[15] In this work, Δ_g refers to a curvature induced band gap in a nominally metallic nanotube, but in the case of a semiconducting nanotube, the dominating band gap E_g, due to a periodic boundary condition around the nanotube circumference should be taken into account.
[16] Including the spin-orbit effect adds a term $s\tau\Delta_{\mathrm{SO}}/2$ with the effective spin-orbit coupling $\Delta_{\mathrm{SO}} = 2(\Delta^0_{\mathrm{SO}} \mp \frac{\Delta^1_{\mathrm{SO}}}{\sqrt{1+(\frac{\epsilon_N}{\Delta_g})^2}})$, where Δ_0 and Δ_1 are spin-orbit parameters related to the band structure.
[17] W. Liang, M. Bockrath, and H. Park, Phys. Rev. Lett. **88**, 126801 (2002).

[18] D. H. Cobden and J. Nygård, Phys. Rev. Lett. **89**, 046803 (2002).
[19] S. Weiss *et al.*, Phys. Rev. B **82**, 165427 (2010).
[20] Attocube ANRv51/res.
[21] L. Kouwenhoven, D. Austing, and S. Tarucha, Rep. Prog. Phys. **64**, 701 (2001).
[22] In Figs. 3(b)–3(d), an overall shift of the gate-position of the diamond has been subtracted to reveal the relative shifts of the excited states with respect to the ground state.
[23] See Supplemental Material at http://link.aps.org/supplemental/10.1103/PhysRevLett.107.186802 for additional data.
[24] From the measured 8 shells per 1 V gate voltage and an average level spacing of 3.1 meV measured at large filling when $\Delta E \approx \hbar v_F \pi / L = \epsilon_N / N$ we estimate $\varepsilon_N \approx (25\ \mathrm{meV/V}) V_g$.
[25] P. Jarillo-Herrero *et al.*, Nature (London) **429**, 389 (2004).
[26] P. Jarillo-Herrero *et al.*, Phys. Rev. Lett. **94**, 156802 (2005).
[27] A. Makarovski *et al.*, Phys. Rev. B **75**, 241407 (2007).
[28] H. Churchill *et al.*, Phys. Rev. Lett. **102**, 166802 (2009).
[29] V. Deshpande and M. Bockrath, Nature Phys. **4**, 314 (2008).
[30] D. C. Elias *et al.*, Nature Phys. **7**, 701 (2011).
[31] S. G. Lemay *et al.*, Nature (London) **412**, 617 (2001).
[32] K. Chuang *et al.*, Phil. Trans. R. Soc. A **366**, 237 (2008).
[33] J. Cao *et al.*, Phys. Rev. Lett. **93**, 216803 (2004).